

Redistributing the energy flow of tightly focused ellipticity-variant vector optical fields

XU-ZHEN GAO,¹ YUE PAN,¹ GUAN-LIN ZHANG,¹ MENG-DAN ZHAO,¹ ZHI-CHENG REN,¹ CHEN-GHOU TU,¹ YONG-NAN LI,^{1,3} AND HUI-TIAN WANG^{1,2,*}

¹School of Physics and Key Laboratory of Weak-Light Nonlinear Photonics, Nankai University, Tianjin 300071, China

²National Laboratory of Solid State Microstructures, School of Physics, and Collaborative Innovation Center of Advanced Microstructures, Nanjing University, Nanjing 210093, China

³e-mail: liyongnan@nankai.edu.cn

*Corresponding author: htwang@nju.edu.cn

Received 27 June 2017; revised 15 September 2017; accepted 29 September 2017; posted 2 October 2017 (Doc. ID 301109); published 31 October 2017

The redistribution of the energy flow of tightly focused ellipticity-variant vector optical fields is presented. We theoretically design and experimentally generate this kind of ellipticity-variant vector optical field, and further explore the redistribution of the energy flow in the focal plane by designing different phase masks including fanlike phase masks and vortex phase masks on them. The flexibly controlled transverse energy flow rings of the tightly focused ellipticity-variant vector optical fields with and without phase masks can be used to transport multiple absorptive particles along certain paths, which may be widely applied in optical trapping and manipulation. © 2017 Chinese Laser Press

OCIS codes: (260.0260) Physical optics; (260.5430) Polarization.

<https://doi.org/10.1364/PRJ.5.000640>

1. INTRODUCTION

During the past few years, manipulation of polarization has become a rather appealing and promising topic of physical optics. The polarization as an additional degree of freedom can be used to control light, leading to the creation of vector optical fields (VOFs) with spatially inhomogeneous states of polarization (SoPs) [1,2]. Due to the unique polarization distribution, the VOFs have exhibited great potential in a variety of scientific and engineering applications, such as nonlinear optics [3–5], quantum optics and information [6,7], optical imaging [8], near-field optics [9], and optical trapping and manipulation of particles [10,11]. The energy flow in the focal plane of the optical field is always interesting and useful, as it can be widely used in optical trapping and manipulation [12,13]. One interesting idea is to study the energy flow of tightly focused VOFs [14–17], taking full advantage of the flexibly controlled space-variant distribution of polarization. As is known, the transversal Poynting vector of the frequently used focused cylindrical vector field is always zero, and there are only a few reports about redistributing the transverse energy flow of the cylindrical vector fields with amplitude and phase modulation [14,17]. To our knowledge, there is no work related to the energy flow of tightly focused vector fields without cylindrical symmetry. Hence, it is necessary to discover the transverse energy flow of new kinds of VOFs, and the impact of

modulation masks on the designing of energy flow is also worth investigating.

In this paper, we study the redistribution of the energy flow in the focal plane of one specific kind of VOF called the ellipticity-variant VOF (EV-VOF). We theoretically design and experimentally generate EV-VOFs, and the polarization of the EV-VOF has the space-invariant orientation of the long axis and space-variant ellipticity, which is very different from the previously existing VOFs [1,2,18–21]. The expression for the electromagnetic fields and Poynting vector in the focal plane based on the vectorial Richards–Wolf diffraction integration is presented, and the transverse energy flow of the tightly focused EV-VOFs can transport multiple absorptive particles to fixed locations. We also add two kinds of phase masks to the EV-VOFs in order to gain various energy flow rings in the focal plane. As a result, the absorptive particles can be transported along flexibly controlled paths at uniform and nonuniform speeds.

2. EV-VOF

We utilize the Poincaré sphere (PS) to deduce the SoPs of the EV-VOF. The PS representation of polarization states of light is shown in Fig. 1(a), and the coordinates 2α and 2ϕ on the PS stand for the latitude and longitude angles, respectively, of a point in a spherical coordinate system. The SoP at a given point

$(2\phi, 2\alpha)$ on the PS can be described by the unit vector $\hat{S}(2\phi, 2\alpha)$ as follows [22]:

$$\begin{aligned}\hat{S}(2\phi, 2\alpha) &= \begin{bmatrix} \sin(\alpha + \pi/4) \exp(-j\phi) \hat{e}_r \\ \cos(\alpha + \pi/4) \exp(j\phi) \hat{e}_t \end{bmatrix} \\ &= \begin{bmatrix} \cos\alpha(\cos\phi \hat{e}_x + \sin\phi \hat{e}_y) \\ j\sin\alpha(-\sin\phi \hat{e}_x + \cos\phi \hat{e}_y) \end{bmatrix},\end{aligned}\quad (1)$$

where $\{\hat{e}_r, \hat{e}_t\}$ are right-handed (RH) and left-handed (LH) unit circular vectors, respectively, while $\{\hat{e}_x, \hat{e}_y\}$ are orthogonal base vectors in the Cartesian coordinate system. The orientation of polarization controlled by ϕ changes along the longitude of the PS, while the ellipticity of polarization controlled by α changes along the latitude. To guarantee an EV-VOF with only one orientation of polarization, we should design and construct this new kind of VOF along one single longitude of the PS. From the north pole to the south pole of the PS in Fig. 1(a), the polarization changes through this progress, from right circular polarization (north pole A) to right elliptical polarization to linear polarization (the equator) to left elliptical polarization to left circular polarization (south pole B). All the polarizations occurring in the EV-VOF we designed are along this single longitude, including linear, elliptical, and circular polarizations.

Here we define the ellipticity of polarization as

$$\varepsilon = \sin(2\alpha), \quad (2)$$

where 2α is the latitude of the PS, with $\alpha \in [-\pi/4, \pi/4]$. The definition of ellipticity specifies not only the magnitude of ellipticity, $|\varepsilon|$, but also the sense of the elliptical polarization. The positive and negative ε correspond to the RH and LH polarizations, respectively. Particularly, $|\varepsilon| = 1$ and $|\varepsilon| = 0$ stand for the circular and linear polarizations, respectively.

In theory, the ellipticity can take any value or function in the range of $[-1, 1]$ for the EV-VOFs, as the range of α is $[-\pi/4, \pi/4]$. In this paper, we explore two basic kinds of EV-VOFs with the sine form varying ellipticity over a range of $[-1, 1]$ and $[0, 1]$ as

$$\varepsilon_A = \sin[\delta(\phi, r) - \pi/2], \quad (3)$$

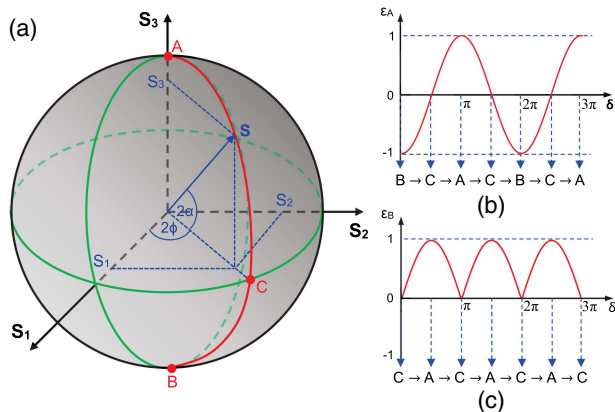


Fig. 1. (a) Schematic of the PS in the spherical coordinate system represented by the traditional latitude and longitude circles and (b) the sine-form varying ellipticity ε_A in a range of $[-1, 1]$ along δ , (c) the sine-form varying ellipticity ε_B in a range of $[0, 1]$ along δ .

$$\varepsilon_B = |\sin[\delta(\phi, r)/2]|, \quad (4)$$

where $\delta(\phi, r)$ is allowed to have an arbitrary spatial distribution. We can see from Eqs. (3) and (4) that ε_A and ε_B are both represented by the sine function and constructed along one longitude of the PS, but the range of the ellipticity is different. The range of ε_A is $[-1, 1]$ and that of ε_B is $[0, 1]$ when $\delta(\phi, r)$ changes from 0 to 2π , as shown in Figs. 1(b) and 1(c). For one period of ε_A , the polarization changes from the south pole (point B) to the north pole (point A), and then from the north pole (point A) to the south pole (point B). However, the polarization changes from the equator (point C) to the north pole (point A), and then from the north pole (point A) to the equator (point C) for one period of ε_B . If we add a minus sign before the expression of ε_B , the polarization of the EV-VOF changes along the longitude below the equator, which is contrary to Fig. 1(c).

The experimental setup for generating the EV-VOFs is shown in Fig. 2, which is a common-path interferometric configuration with the aid of a $4f$ system, based on the wavefront reconstruction and the PS [2,23]. This scheme is a universal method for generating various vector fields. An input linearly polarized light delivered from a laser (Verdi V5, Coherent Inc.) is split into two parts, which are achieved by the first orders diffracted from the sine/cosine grating displayed on a phase-only spatial light modulator (SLM) placed in the input plane of the $4f$ system. The two orders are allowed to pass through a spatial filter (with two separate open apertures) placed at the Fourier plane of the first $4f$ system, and then are converted into two orthogonally polarized beams by a pair of half-wave plates behind the spatial filter. The two orthogonally polarized parts are recombined by the Ronchi phase grating placed in the output plane of the $4f$ system. For the EV-VOFs with the x -oriented polarization ($\phi = 0$), which we concentrate on, the phase function of the holographic grating displayed on the SLM is $t(x, y) = 0.5 + 0.5 \cos\{2\pi f_0 x + \arcsin[\varepsilon(x, y)]\}$, and the SoP of the generated EV-VOF can be represented as

$$\begin{aligned}\mathbf{E} &= \cos\alpha \hat{e}_x + j \sin\alpha \hat{e}_y \\ &= \cos\left[\frac{\sin^{-1}\varepsilon(x, y)}{2}\right] \hat{e}_x + j \sin\left[\frac{\sin^{-1}\varepsilon(x, y)}{2}\right] \hat{e}_y.\end{aligned}\quad (5)$$

When the space-variant ellipticity in Eqs. (3) and (4) is applied, the EV-VOFs with the sine-form varying ellipticity can be presented. We will now demonstrate experimentally the generation of EV-VOFs using the method mentioned above. If we set $\delta(\phi, r)$ in Eqs. (3) and (4) as $\delta(\phi, r) = m\phi + 2\pi n\tau$ in the polar coordinate system, the ellipticity changes

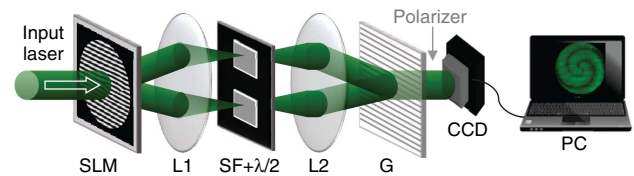


Fig. 2. Schematic of the experimental setup for generating the desired EV-VOFs. L1 and L2, a pair of lenses; $\lambda/2$, half-wave plates; SF, spatial filter; G, Ronchi phase grating; PC, computer.

along the radial and azimuthal directions with cylindrical symmetry. Actually, we can also represent the ellipticity in other coordinates or expressions [21,24], indicating the flexibility of this new kind of EV-VOF.

Figures 3 and 4 show the generated EV-VOFs with the sine-form varying ellipticity in a range of $[-1, 1]$ and $[0, 1]$, respectively, corresponding to Figs. 1(b) and 1(c). The total intensity patterns in the first row exhibit a uniform distribution and have no clear polarization singularity for both cases, which is very different from traditional cylindrical VOFs [1,2,6,7,23]. It is obvious that there is no complete extinction (with zero minimum intensity) in the x -component intensity patterns, which is also different from the traditional cylindrical VOFs.

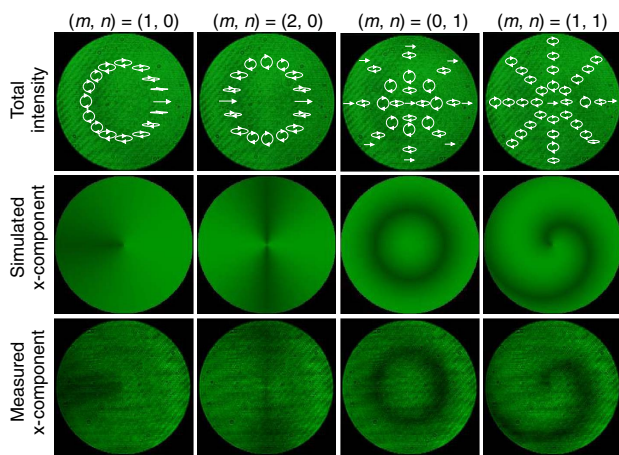


Fig. 3. Generated EV-VOFs when $(m, n) = (1, 0)$, $(2, 0)$, $(0, 1)$, and $(1, 1)$. The first row gives the total intensity patterns and corresponding schematics of the SoPs, and the second and third rows show the simulated and measured x -component intensity patterns, respectively, for the EV-VOFs with the sine-form varying ellipticity in a range of $[-1, 1]$.

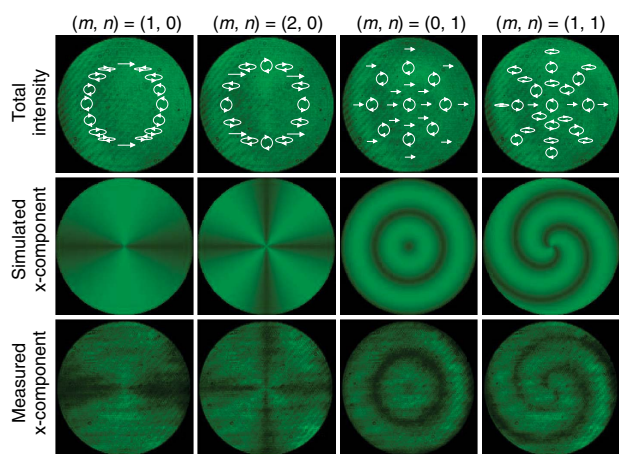


Fig. 4. Generated EV-VOFs when $(m, n) = (1, 0)$, $(2, 0)$, $(0, 1)$, and $(1, 1)$. The first row gives the total intensity patterns and corresponding schematics of the SoPs, and the second and third rows show the simulated and measured x -component intensity patterns, respectively, for the EV-VOFs with the sine-form varying ellipticity in a range of $[0, 1]$.

The simulated x -component intensity patterns in the second row are in good agreement with the measured ones in the third row. First, we discuss the case of EV-VOFs with the sine-form varying ellipticity in a range of $[-1, 1]$, as shown in Fig. 3. When $n = 0$, the ellipticity of the EV-VOF changes along the azimuthal direction; that is to say, the SoP changes along the azimuthal direction. The x -component intensity patterns exhibit fanlike half-extinctions whose maximum intensity is the same as the total intensity, while the minimum intensity is half of the maximum intensity, which means the visibility of the x -component intensity pattern is $1/3$. The positions of the half-extinctions correspond to the positions of the circular polarization, which are also the positions of $|\epsilon_A| = 1$ in Fig. 1(b), so the number of half-extinctions is 2 times of the value of m . When $m = 0$, the ellipticity of the EV-VOF changes along the radial direction, as shown in the third column in Fig. 3. When $n = 1$, the x -component intensity pattern exhibits a ring (corresponding to right circular polarization) and a singularity in the center (corresponding to left circular polarization). When n increases, there is always one singularity in the center, and the number of the half-extinction rings is $2n - 1$. When $(m, n) = (1, 1)$, the ellipticity changes along both azimuthal and radial directions, and the x -component intensity pattern exhibits a spiral shape. In the case of EV-VOFs with the sine-form varying ellipticity in range of $[0, 1]$ in Fig. 4, corresponding to Fig. 1(c), the length of the path that ϵ_B passes on the PS is half of ϵ_A , so the number of fanlike half-extinctions when $n = 0$ is m . When $m = 0$, the x -component intensity pattern exhibits a ring without a singularity in the center, because the polarization in the center is x polarization. We can see that the number of ring-shaped half-extinctions when $m = 0$ is n . When $m \neq 0$ and $n \neq 0$, the x -component intensity pattern exhibits a pair of twisted spirals. As for the y -component intensity patterns of the EV-VOFs whose maximum intensity is half of the total intensity, the intensity patterns exhibit complete extinctions, which are complementary to those of the x component shown in Figs. 3 and 4.

It is worth mentioning that the polarization of the EV-VOFs we design and generate is x -oriented polarization with space-variant ellipticity, but the orientation can actually be arbitrarily designed in the same way we introduced above. We should also state that though the mathematical representation and experimental realization of the EV-VOFs are similar to the previous vector fields with hybrid SOPs [23], the EV-VOF is still a new kind of vector field constructed along only one longitude of the PS, which is very different from all the previously existing kinds of VOFs. Specifically, no matter what the topological charge (m, n) is, there is never complete extinction for the x -component intensity pattern of the EV-VOF, while complete extinction appears for the y -component intensity pattern. Moreover, the proportion of the x component of the EV-VOF is much larger than the y component. Although the EV-VOF is (to our knowledge) a new kind of VOF with some unique properties, it is obvious that the presentation of a new vector field is not enough, as novel properties and useful applications are always expected. Indeed, we design and construct this new kind of EV-VOF during the study of the energy flow of tightly

focused vector fields, so redistributing the energy flow of the EV-VOF will be investigated next.

3. CALCULATION OF ENERGY FLOW IN THE FOCAL PLANE

The study of energy flow in the focal plane of VOFs has always attracted research interest, especially for the local linearly polarized VOFs [14–17]. The most representative application of the energy flow is manipulating and transporting absorptive particles [25–27]. Absorptive particles suspended in water are optically trapped within a laser beam strongly focused by the microscope objective. In absorbing a certain portion of the beam energy, the particles simultaneously obtain the associated portion of its energy flow. This causes the motion of the particles that can be seen by the microscope. For absorbing particles, the trajectory of the particle motion coincides in direction with the Poynting vector, and the velocities of the particle motion along the lines of the Poynting vector are proportional to its modulus. As a result, the energy flow can be seen via the particle trajectory within the beam “body” [28]. We now investigate the distribution of the energy flow,

especially the transverse energy flow, which is useful in manipulating absorptive particles, for a tightly focused EV-VOF.

According to the vectorial Richards–Wolf diffraction integration [29,30], we first derive the electric field expression of a tightly focused EV-VOF as follows:

$$\mathbf{E} = \int_0^{\theta_m} \int_0^{2\pi} P(\theta) \mathbf{M}_e K(\phi, \theta) \sin\theta d\phi d\theta, \quad (6)$$

$$\mathbf{M}_e = \begin{bmatrix} (E_\rho \cos\theta \cos\phi - E_\phi \sin\phi) \hat{\mathbf{e}}_x \\ (E_\rho \cos\theta \sin\phi + E_\phi \cos\phi) \hat{\mathbf{e}}_y \\ E_\rho \sin\theta \hat{\mathbf{e}}_z \end{bmatrix}, \quad (7)$$

$$K(\phi, \theta) = e^{jk[z\cos\theta + r\sin\theta\cos(\phi-\phi)]}, \quad (8)$$

where ρ and ϕ are the radial and azimuthal coordinates, respectively, and E_ρ and E_ϕ are the radial and azimuthal components, respectively, of the incident vector fields in the polar coordinate system (ρ, ϕ) on the input plane. r , φ , and z are the radial, azimuthal, and longitudinal coordinates, respectively, in the cylindrical coordinate system (r, φ, z) on the focal plane. $k = 2\pi/\lambda$ is the wavenumber, and λ is the wavelength in free

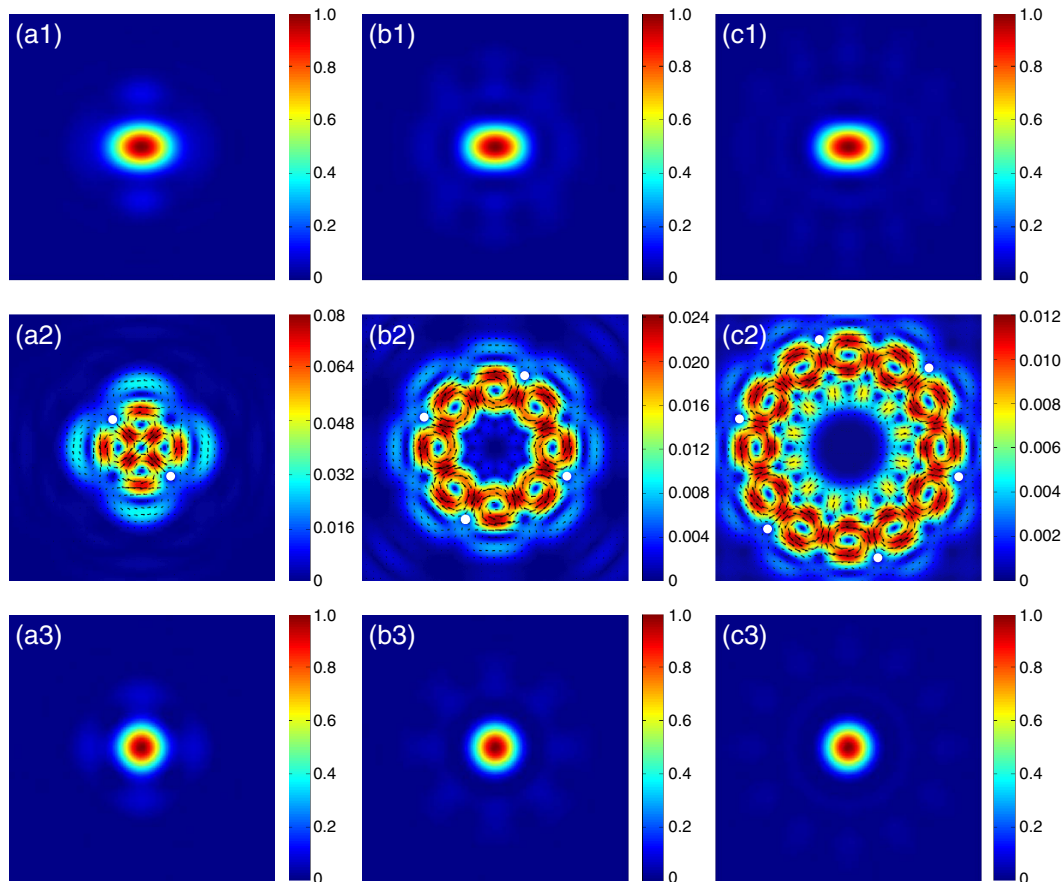


Fig. 5. Intensity distributions and the Poynting vectors in the focal plane of the tightly focused EV-VOFs with the sine-form varying ellipticity in a range of $[-1, 1]$ when $(m, n) = (2, 0)$, $(4, 0)$, and $(6, 0)$ (left, middle, and right columns, respectively). The intensity patterns of the tightly focused fields are shown in the first row, and the transverse and longitudinal components of the normalized Poynting vectors in the focal plane are shown in the second and third rows, respectively. The direction of the transverse energy flow is shown by the black arrows. All images have dimensions of $4\lambda \times 4\lambda$.

space. $P(\theta)$ is the pupil plane apodization function, and \mathbf{M}_e is the electric polarization vector in the tightly focused field.

As is well known, the electric and magnetic vectors are orthogonal in an isotropic dielectric [15,29], and they satisfy the relations $\mathbf{M}_m = \mathbf{k} \times \mathbf{M}_e$, where $\mathbf{k} = (-\sin\theta\cos\phi, -\sin\theta\sin\phi, \cos\theta)$ is the unit vector of the wave vector. The magnetic field of a highly focused EV-VOF can be described by

$$\mathbf{H} = \int_0^{\theta_m} \int_0^{2\pi} P(\theta)\mathbf{M}_m K(\phi, \theta) \sin\theta d\phi d\theta, \quad (9)$$

$$\mathbf{M}_m = \begin{bmatrix} (-E_\rho \sin\phi - E_\phi \cos\theta \cos\phi)\hat{\mathbf{e}}_x \\ (E_\rho \cos\phi - E_\phi \cos\theta \sin\phi)\hat{\mathbf{e}}_y \\ -E_\phi \sin\theta \hat{\mathbf{e}}_z \end{bmatrix}. \quad (10)$$

We can see that the distribution of the magnetic polarization vector in Eq. (10) is different from that of the electric polarization vector in Eq. (7). In terms of the full time-dependent three-dimensional electric and magnetic field vectors, the energy current can be defined by the time-averaged Poynting vector [12–15,17,31]:

$$\mathbf{P} \propto \text{Re}[\mathbf{E}^* \times \mathbf{H}] \propto \text{Im}[(\mathbf{E}^* \cdot \nabla)\mathbf{E}] + \frac{1}{2}\nabla \times \text{Im}(\mathbf{E}^* \times \mathbf{E}), \quad (11)$$

where \mathbf{E} and \mathbf{H} are the electric and magnetic fields in the focal plane, respectively, the scalar product (\cdot) links the vectors \mathbf{E}^* and \mathbf{E} , and ∇ represents the well-known gradient operator. We can calculate the energy flow of tightly focused EV-VOFs with Eqs. (6)–(11), and the numerical aperture is $\text{NA} = 0.95$ in the following calculations.

Now we discuss the energy flow of the EV-VOFs with the sine-form varying ellipticity in a range of $[-1, 1]$ —in particular, the transverse energy flow for manipulating the absorptive particles. By calculation, we find that the transverse energy flow is zero in the case of an odd topological charge m , while the transverse energy flow exists in the case of an even topological charge m . The intensity and the Poynting vectors of the tightly focused fields in the focal plane when $m = 2, 4,$ and 6 are shown in Fig. 5, and the intensity pattern of the tightly focused field always exhibits an ellipse shape. This elliptical focal spot is similar to the tightly focused field of the linearly polarized field [32,33], because the proportion of the x component of the EV-VOF we study is always large. We can see in Fig. 5(a2) that when $m = 2$, there are four transverse energy flow rings, and two of them are clockwise while the other two

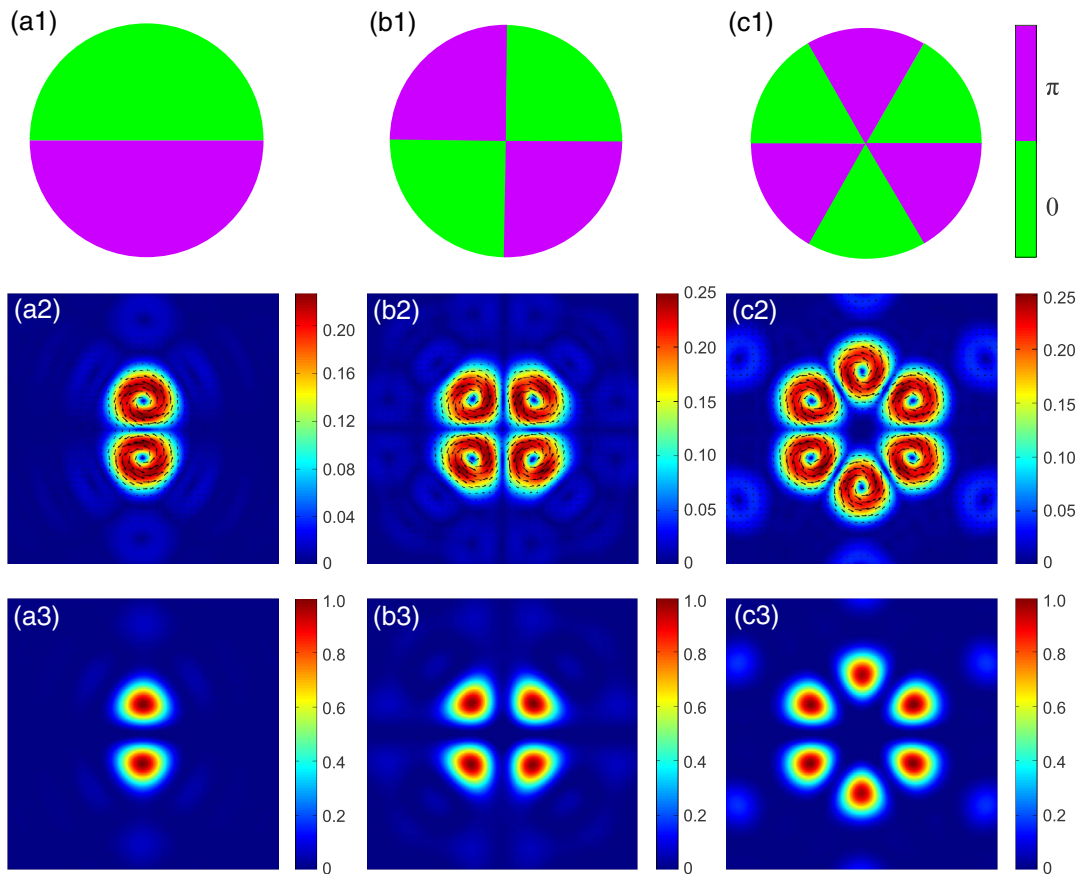


Fig. 6. Schematic structures of the phase masks and the Poynting vectors of the tightly focused EV-VOFs with the sine-form varying ellipticity in a range of $[0, 1]$ when $(m, n) = (1, 0)$. The cases of twofold, fourfold, and sixfold fanlike phase masks are shown in the first, second, and third columns, respectively. The schematics of fanlike phase masks are shown in the first row, and the transverse and longitudinal components of the normalized Poynting vectors in the focal plane are shown in the second and third rows, respectively. The direction of the transverse energy flow is shown by the black arrows. All images in the second and third rows have dimensions of $4\lambda \times 4\lambda$.

are counterclockwise. The energy finally flows to two fixed locations marked by two white points, which means the absorptive particles can be transported to the fixed locations along different routes. As the topological charge m increases, the number of energy flow rings increases correspondingly. The number of energy flow rings is $2m$, and the number of fixed manipulating locations (white points) is m , as shown in Figs. 5(b2) and 5(c2), respectively. However, the magnitude of the transverse component of the Poynting vector, compared with the z component, will gradually decrease as m increases, and thus it becomes more difficult to manipulate particles in the transverse plane.

4. PHASE MASKS AND REDISTRIBUTION OF THE ENERGY FLOW

Recently, due to the increasing interest in the study of VOFs modulated by phase masks [14,17,34], two types of phase modulation, fanlike phase masks and vortex phase masks, are applied to EV-VOFs to investigate the energy flow in the focal plane. Figure 6 shows the energy flow in the focal plane of the EV-VOFs modulated by fanlike phase masks with different phase retardation in different regions. The three rows in Fig. 6 display the phase masks and the transverse and longitudinal components of the Poynting vectors in the focal plane of the tightly focused EV-VOFs with the sine-form varying ellipticity in a range of $[0, 1]$ when $m = 1$. The first column

in Fig. 6 depicts the energy flow for the phase mask shown in Fig. 6(a1), which is composed of an upper half with 0 phase retardation and a bottom half with π phase retardation. It can be seen from the corresponding transverse energy flow that two counterclockwise transverse energy flow rings play the dominant role, which can be used to trap and transport two absorptive particles in different circles. The second and third columns show the energy flow in the focal plane for fourfold and sixfold phase masks, and the transverse energy flows exhibit four and six counterclockwise energy flow rings, respectively, as shown in Figs. 6(b2) and 6(c2). The number of transverse energy flow rings is equal to the number of regions of the phase mask, and the number of symmetric axes of the Poynting vectors is also equal to the number of regions of the phase mask. We can also see in Fig. 6 that the transverse energy flow rings exhibit approximately fanlike shapes, similar to the phase masks.

As we have shown in Fig. 6, a different number of transverse energy flow rings can be gained by changing to different fanlike phase masks. In addition, Fig. 7 shows how to change the locations of the transverse energy flow rings by rotating the phase mask by an angle of $0, \pi/4, \pi/2,$ and $3\pi/4$, respectively. We can see in Fig. 7 that the transverse energy flow rotates by the same angle as the corresponding phase mask. As a result, we can control the location of each transverse energy flow ring by simply rotating the fanlike phase mask, which provides more degrees of freedom to transport multiple particles.

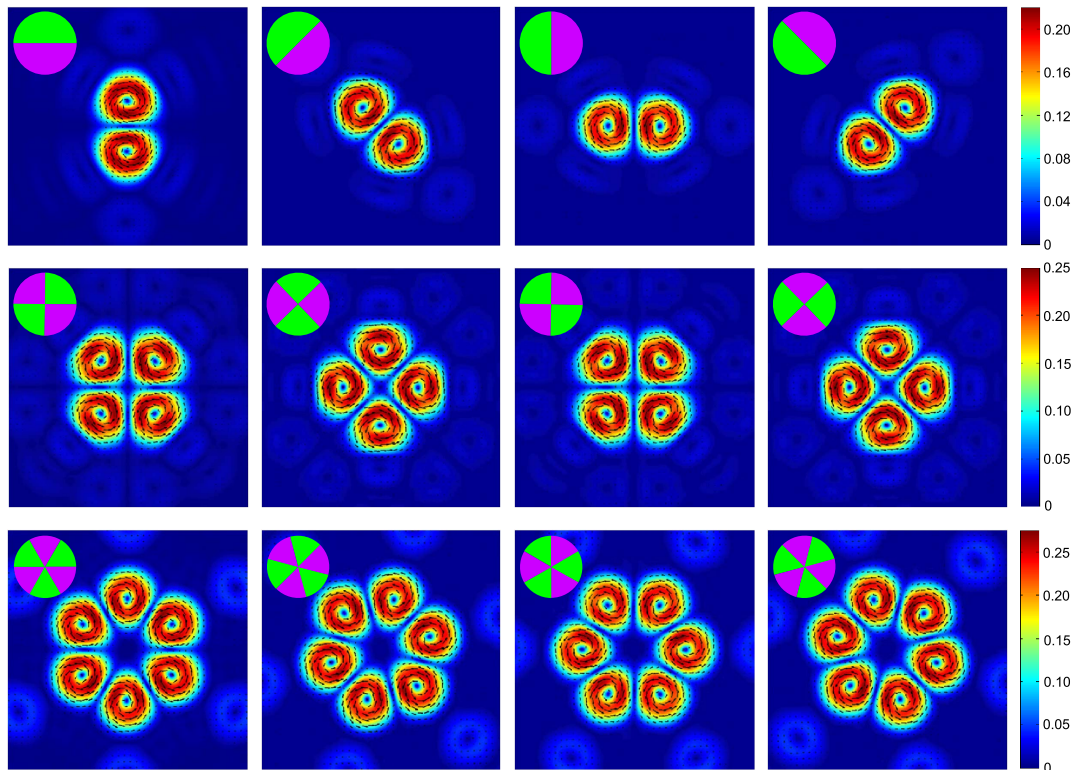


Fig. 7. Transverse components of the Poynting vectors of the tightly focused EV-VOFs with the sine-form varying ellipticity in a range of $[0, 1]$ when $(m, n) = (1, 0)$. The cases of twofold, fourfold, and sixfold fanlike phase masks are shown in the first, second, and third rows, respectively. The rotation angles of the phase masks in columns 1–4 are $0, \pi/4, \pi/2,$ and $3\pi/4$, respectively. The insets show the corresponding fanlike phase masks used. The direction of the transverse energy flow is shown by the black arrows. All images have dimensions of $4\lambda \times 4\lambda$.

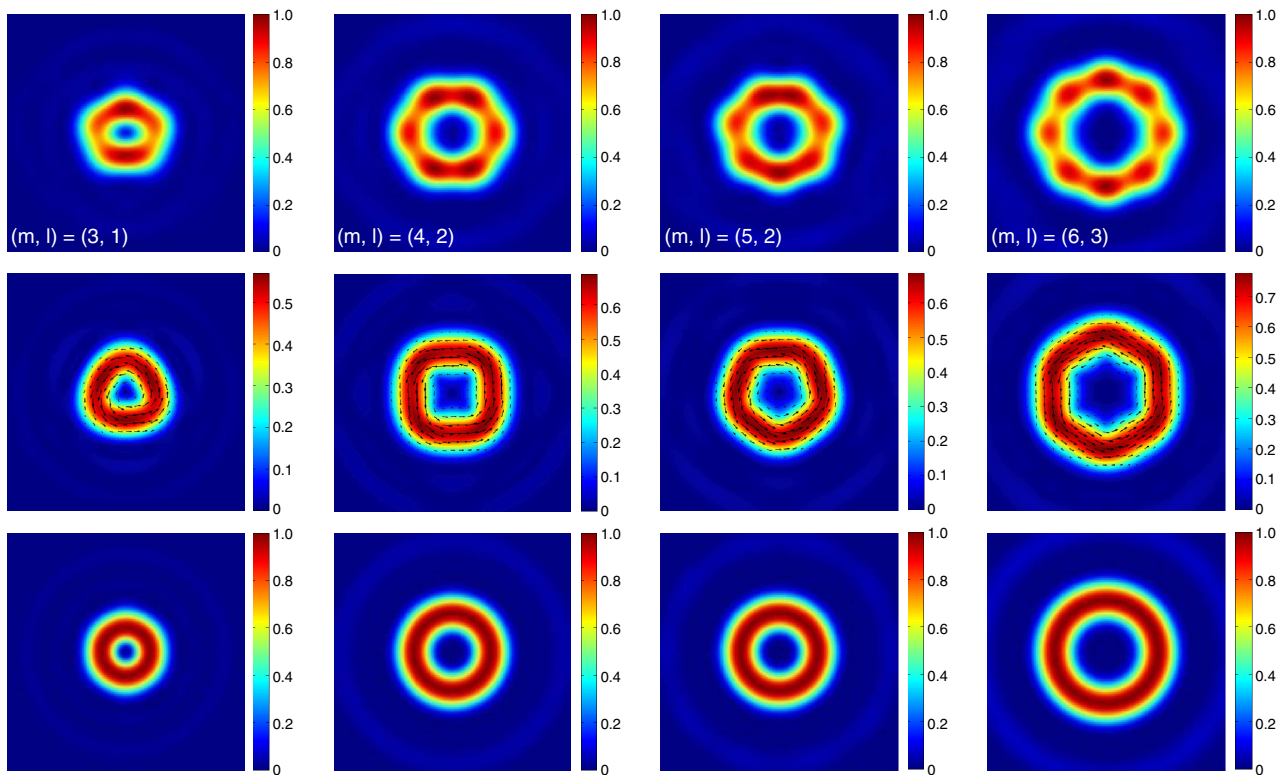


Fig. 8. Intensity distributions and the Poynting vectors of the tightly focused vortex EV-VOfs with the sine-form varying ellipticity in a range of $[0, 1]$ when $(m, l) = (3, 1), (4, 2), (5, 2),$ and $(6, 3)$ (columns 1–4, respectively). The intensity patterns of the tightly focused fields are shown in the first row, and the transverse and longitudinal components of the normalized Poynting vectors in the focal plane are shown in the second and third rows, respectively. The direction of the transverse energy flow is shown by the black arrows. All images have dimensions of $4\lambda \times 4\lambda$.

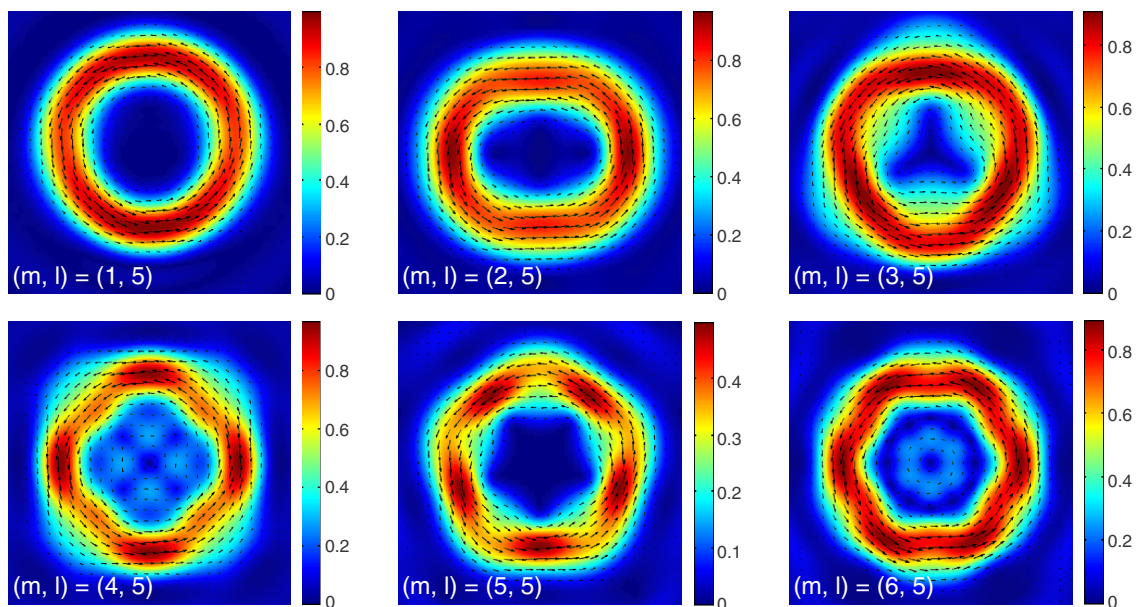


Fig. 9. Transverse components of the normalized Poynting vectors of the tightly focused vortex EV-VOfs with the sine-form varying ellipticity in a range of $[-1, 1]$ when $(m, l) = (1, 5), (2, 5), (3, 5), (4, 5), (5, 5),$ and $(6, 5)$. The direction of the transverse energy flow is shown by the black arrows. All images have dimensions of $4\lambda \times 4\lambda$.

VOFs with a vortex phase are called vortex VOFs, and they have attracted much attention [35,36]. We simulate the energy flow of tightly focused vortex EV-VOFs with the sine-form varying ellipticity in a range of [0, 1], as shown in Fig. 8. The first row in Fig. 8 displays the intensity of the tightly focused fields when $(m, l) = (3, 1), (4, 2), (5, 2),$ and $(6, 3)$, where l is the topological charge of the vortex phase. The second and third rows show the transverse and longitudinal components, respectively, of the Poynting vectors of the tightly focused vortex EV-VOFs. It can be seen that the profiles of the transverse components of the Poynting vectors are polygons: a triangle, quadrangle, pentagon, and hexagon, respectively. The number of the sides of the polygon is equal to the polarization topological charge m , and the absorptive particles can be transported along the polygon in the transverse plane. To get a more standard and uniform polygon of the transverse energy flow, the proper topological charge l is chosen to match the value of m in Fig. 8. We should also point out that when l increases, the proportion of the transverse energy flow will gradually increase, and the size of the polygon of the transverse energy flow will also increase. The longitudinal components of the Poynting vectors in Fig. 8 are always circles, with the radius dependent on l instead of m . Although the absorptive particles cannot move exactly along the path of the polygon, we are still interested in designing the uniform transverse energy flow to transport the absorptive particles along a certain path at an approximate uniform speed.

Figure 9 shows another case of the transverse energy flows of tightly focused vortex EV-VOFs with the sine-form varying ellipticity in a range of $[-1, 1]$. In this case, the polygon-shaped transverse energy flows are not uniform anymore. When $m = 1$, the energy converges on the upper and lower sides of the approximately circular transverse energy flow ring. The energy flow ring becomes elliptical when $m = 2$, and the energy converges on the left and right sides. As m increases from 3 to 6, the energy converges on 3 to 6 points on the transverse energy flow, which creates a polygon shape with 3 to 6 sides. Obviously, the absorptive particles can be transported at a nonuniform speed by the transverse flows, as shown in Fig. 9, which also demonstrates the flexibility in controlling the transverse energy flows of tightly focused EV-VOFs.

Based on the variety of energy flow patterns presented, we further summarize a detailed procedure for controlling energy flow. By adjusting the distribution of the phase and polarization, the distribution of the energy flow can be controlled conveniently and flexibly. In theory, we should calculate the energy flow using Eqs. (6)–(11), and it is essential to consider the symmetry of the SoPs of the EV-VOFs, the value of the topological charge of the EV-VOFs, the different choices of phase masks, and so on. For experimental generation, the setup shown in Fig. 2 can be applied to generate arbitrary EV-VOFs, and various kinds of phase masks can be added to modulate the phase distribution. As a matter of fact, there have been mature techniques similar to the method shown in Fig. 2 for generating optical fields with arbitrary polarization and phase distributions [37,38], which can be applied to directly generate EV-VOFs with an arbitrary phase distribution. With these theories and experimental methods, we believe various kinds of energy flows can be designed and generated.

5. CONCLUSIONS

In summary, we have proposed theoretically and generated experimentally a new (to our knowledge) kind of EV-VOF, which is constructed on one longitude of the PS, so the orientation of polarization is space invariant and the ellipticity of the polarization is space variant. Then we introduced the theory of how to calculate the electromagnetic fields and the energy flow of tightly focused optical fields, and concentrated on the redistribution of the transverse energy flow of the tightly focused EV-VOFs, which can transport absorptive particles to fixed locations. When fanlike phase masks are added on the EV-VOFs, flexibly controlled transverse energy flow rings can be gained in the focal plane. Another kind of common phase masks is the vortex phase mask, with which we can get uniform and non-uniform transverse energy flows with the shapes of different polygons. All these flexibly controlled transverse energy flow rings can transport multiple absorptive particles along certain paths or to fixed locations, which means multiple particles can be trapped and transported via the redistribution of the transverse energy flow of tightly focused EV-VOFs.

Funding. National Natural Science Foundation of China (NSFC) (11374166, 11534006, 11674184); National key research and development program of China (2017YFA0303700, 2017YFA0303800); Natural Science Foundation of Tianjin City (16JC2DJC31300).

Acknowledgment. This work is supported by the Collaborative Innovation Center of Extreme Optics.

REFERENCES

1. Q. Zhan, "Cylindrical vector beams: from mathematical concepts to applications," *Adv. Opt. Photon.* **1**, 1–57 (2009).
2. X. L. Wang, J. P. Ding, W. J. Ni, C. S. Guo, and H. T. Wang, "Generation of arbitrary vector beams with a spatial light modulator and a common path interferometric arrangement," *Opt. Lett.* **32**, 3549–3551 (2007).
3. A. Bouhelier, M. Beversluis, A. Hartschuh, and L. Novotny, "Near-field second-harmonic generation induced by local field enhancement," *Phys. Rev. Lett.* **90**, 013903 (2003).
4. S. Sato and Y. Kozawa, "Radially polarized annular beam generated through a second-harmonic-generation process," *Opt. Lett.* **34**, 3166–3168 (2009).
5. S. M. Li, Y. Li, X. L. Wang, L. J. Kong, K. Lou, C. Tu, Y. Tian, and H. T. Wang, "Taming the collapse of optical fields," *Sci. Rep.* **2**, 1007 (2012).
6. J. T. Barreiro, T. C. Wei, and P. G. Kwiat, "Remote preparation of single-photon 'hybrid' entangled and vector-polarization states," *Phys. Rev. Lett.* **105**, 030407 (2010).
7. C. Gabriel, A. Aiello, W. Zhong, T. G. Euser, N. Y. Joly, P. Banzer, M. Förtsch, D. Elser, U. L. Andersen, C. Marquardt, P. St. J. Russell, and G. Leuchs, "Entangling different degrees of freedom by quadrature squeezing cylindrically polarized modes," *Phys. Rev. Lett.* **106**, 060502 (2011).
8. F. Lu, W. Zheng, and Z. Huang, "Coherent anti-Stokes Raman scattering microscopy using tightly focused radially polarized light," *Opt. Lett.* **34**, 1870–1872 (2009).
9. A. Ciattoni, B. Crosignani, P. Di Porto, and A. Yariv, "Azimuthally polarized spatial dark solitons: exact solutions of Maxwell's equations in a Kerr medium," *Phys. Rev. Lett.* **94**, 073902 (2005).
10. Q. Zhan, "Trapping metallic Rayleigh particles with radial polarization," *Opt. Express* **12**, 3377–3382 (2004).

11. X. L. Wang, J. Chen, Y. N. Li, J. P. Ding, C. S. Guo, and H. T. Wang, "Optical orbital angular momentum from the curl of polarization," *Phys. Rev. Lett.* **105**, 253602 (2010).
12. O. V. Angelsky, A. Y. Bekshaev, P. P. Maksimyak, A. P. Maksimyak, S. G. Hanson, and C. Y. Zenkova, "Orbital rotation without orbital angular momentum: mechanical action of the spin part of the internal energy flow in light beams," *Opt. Express* **20**, 3563–3571 (2012).
13. O. V. Angelsky, A. Y. Bekshaev, P. P. Maksimyak, A. P. Maksimyak, C. Y. Zenkova, and N. V. Gorodyska, "Circular motion of particles by the help of the spin part of the internal energy flow," *Proc. SPIE* **8882**, 88820A (2013).
14. X. Jiao, S. Liu, Q. Wang, X. Gan, P. Li, and J. Zhao, "Redistributing energy flow and polarization of a focused azimuthally polarized beam with rotationally symmetric sector-shaped obstacles," *Opt. Lett.* **37**, 1041–1043 (2012).
15. Y. Zhang and B. Ding, "Magnetic field distribution of a highly focused radially-polarized light beam," *Opt. Express* **17**, 22235–22239 (2009).
16. G. Wu, F. Wang, and Y. Cai, "Generation and self-healing of a radially polarized Bessel–Gauss beam," *Phys. Rev. A* **89**, 043807 (2014).
17. G. H. Yuan, S. B. Wei, and X. C. Yuan, "Generation of nondiffracting quasi-circular polarization beams using an amplitude modulated phase hologram," *J. Opt. Soc. Am. A* **28**, 1716–1720 (2011).
18. S. C. Tidwell, D. H. Ford, and W. D. Kimura, "Generating radially polarized beams interferometrically," *Appl. Opt.* **29**, 2234–2239 (1990).
19. A. M. Beckley, T. G. Brown, and M. A. Alonso, "Full Poincaré beams," *Opt. Express* **18**, 10777–10785 (2010).
20. W. Han, W. Cheng, and Q. Zhan, "Flat-top focusing with full Poincaré beams under low numerical aperture illumination," *Opt. Lett.* **36**, 1605–1607 (2011).
21. G. M. Lerman and U. Levy, "Tight focusing of spatially variant vector optical fields with elliptical symmetry of linear polarization," *Opt. Lett.* **32**, 2194–2196 (2007).
22. M. Born and E. Wolf, *Principles of Optics*, 7th ed. (Cambridge University, 1999).
23. X. L. Wang, Y. N. Li, J. Chen, C. S. Guo, J. P. Ding, and H. T. Wang, "A new type of vector fields with hybrid states of polarization," *Opt. Express* **18**, 10786–10795 (2010).
24. Y. Pan, Y. N. Li, S. M. Li, Z. C. Ren, Y. Si, C. Tu, and H. T. Wang, "Vector optical fields with bipolar symmetry of linear polarization," *Opt. Lett.* **38**, 3700–3703 (2013).
25. A. Bekshaev, M. Soskin, and M. Vasnetsov, *Paraxial Light Beams with Angular Momentum* (Nova Science, 2008).
26. O. V. Angelsky, M. P. Gorsky, P. P. Maksimyak, A. P. Maksimyak, S. G. Hanson, and C. Yu. Zenkova, "Investigation of optical currents in coherent and partially coherent vector fields," *Opt. Express* **19**, 660–672 (2011).
27. M. E. J. Friese, J. Enger, H. Rubinsztein-Dunlop, and N. R. Heckenberg, "Optical angular-momentum transfer to trapped absorbing particles," *Phys. Rev. A* **54**, 1593–1596 (1996).
28. A. Bekshaev, K. Bliokh, and M. Soskin, "Internal flows and energy circulation in light beams," *J. Opt.* **13**, 053001 (2011).
29. B. Richards and E. Wolf, "Electromagnetic diffraction in optical systems II. Structure of the image field in an aplanatic system," *Proc. R. Soc. London A* **253**, 358–379 (1959).
30. K. S. Youngworth and T. G. Brown, "Focusing of high numerical aperture cylindrical-vector beams," *Opt. Express* **7**, 77–87 (2000).
31. M. V. Berry, "Optical currents," *J. Opt.* **11**, 094001 (2009).
32. J. W. M. Chon, X. Gan, and M. Gu, "Splitting of the focal spot of a high numerical-aperture objective in free space," *Appl. Phys. Lett.* **81**, 1576–1578 (2002).
33. R. Dorn, S. Quabis, and G. Leuchs, "The focus of light—linear polarization breaks the rotational symmetry of the focal spot," *J. Mod. Opt.* **50**, 1917–1926 (2003).
34. P. Li, S. Liu, G. Xie, T. Peng, and J. Zhao, "Modulation mechanism of multi-azimuthal masks on the redistributions of focused azimuthally polarized beams," *Opt. Express* **23**, 7131–7139 (2015).
35. X. Hao, C. F. Kuang, T. T. Wang, and X. Liu, "Phase encoding for sharper focus of the azimuthally polarized beam," *Opt. Lett.* **35**, 3928–3930 (2010).
36. D. Zhang, X. Feng, K. Cui, F. Liu, and Y. Huang, "Identifying orbital angular momentum of vectorial vortices with Pancharatnam phase and Stokes parameters," *Sci. Rep.* **5**, 11982 (2015).
37. H. Chen, J. Hao, B. F. Zhang, J. Xu, J. Ding, and H. T. Wang, "Generation of vector beam with space-variant distribution of both polarization and phase," *Opt. Lett.* **36**, 3179–3181 (2011).
38. Z. Chen, T. Zeng, B. Qian, and J. Ding, "Complete shaping of optical vector beams," *Opt. Express* **23**, 17701–17710 (2015).